Unveiling Nanoscale Compositional and Structural Heterogeneities of Highly Textured $Mg_{0.7}Ti_{0.3}H_y$ Thin Films

Kim, Hyunjeong; Schreuders, Herman; Sakaki, Kouji; Asano, Kohta; Nakamura, Yumiko; Maejima, Naoyuki; Machida, Akihiko; Watanuki, Tetsu; Dam, Bernard

DOI
10.1021/acs.inorgchem.0c00059

Publication date
2020

Document Version
Final published version

Published in
Inorganic Chemistry

Inorganic Chemistry

pubs.acs.org/IC Article

Unveiling Nanoscale Compositional and Structural Heterogeneities of Highly Textured $Mg_{0.7}Ti_{0.3}H_y$ Thin Films

Hyunjeong Kim,* Herman Schreuders, Kouji Sakaki, Kohta Asano, Yumiko Nakamura, Naoyuki Maejima, Akihiko Machida, Tetsu Watanuki, and Bernard Dam

Cite This: *Inorg. Chem.* 2020, 59, 6800–6807 Read Online

ACCESS | Metrics & More | Article Recommendations | Supporting Information

ABSTRACT: Thin films often exhibit fascinating properties, but the understanding of the underlying mechanism behind such properties is not simple. This is partially because of the limited structural information available. The hurdle in obtaining such information is especially high for textured thin films such as Mg-rich Mg_xTi_{1-x}, a promising switchable smart coating material. Although these metastable thin films are seen as solid solution alloys by conventional crystallographic methods, their hydrogen-induced optical transition is hardly understood by a solid solution model. In this study, we collect atomic pair distribution function (PDF) data for a $Mg_{0.7}Ti_{0.3}H_y$ thin film in situ on hydrogenation and successfully resolve TiH_2 clusters of an average size of 30 Å embedded in the Mg matrix. This supports the chemically segregated model previously proposed for this system. We also observe the emergence of a previously unknown intermediate face-centered tetragonal phase during hydrogenation of the Mg matrix. This phase appears between Mg and MgH_2 to reduce lattice mismatch, thereby preventing pulverization and facilitating rapid hydrogen uptake. This work may shed new light on the hydrogen-induced properties of Mg-rich Mg_xTi_{1-x} thin films.

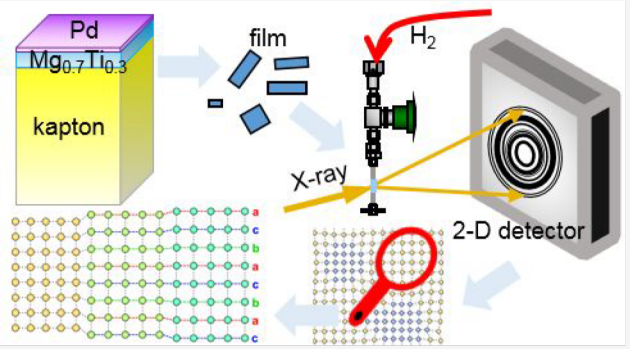

INTRODUCTION

Thin-film deposition is one of the controlled synthesis methods that allow the preparation of materials in unique architectures. For instance, we can bind thin layers of various materials together to make heterogeneous substances or grow metastable materials that do not appear in equilibrium phase diagrams.[1−4] Such thin films often exhibit fascinating properties and hence play an important role in a wide range of applications these days including transparent electronics, memories, optical coatings, and renewable energy,[5−8] and thin film deposition will take on great significance for next-generation functional materials.[9,10] However, the structural determination of thin films, especially on the nanoscale, is not straightforward and this leads to a limited understanding of the properties of thin films.

Mg-rich Mg_xTi_{1-x} thin films prepared by magnetron sputter deposition exhibit interesting hydrogen-induced optical transition properties: a highly reflective metallic film transforms to a strong absorber of solar radiation with a low thermal emissivity by hydrogen absorption.[11] These thin films have a wide range of potential applications such as switchable smart coatings for solar collectors[12,13] and hydrogen sensors.[14] Which structural features give rise to such compelling properties is of great interest. X-ray diffraction (XRD) and selected area electron diffraction studies suggest that Mg_xTi_{1-x} thin films are "solid solution alloys" having a hexagonal-close-packed (hcp) structure and they transform on hydrogenation into face-centered-cubic (fcc)-based hydrides.[15] However, the formation of Mg−Ti solid solutions is questionable because Mg and Ti are immiscible.[16] Moreover, a simple solid solution model does not account for the optical and electrical properties of the hydrogenated thin films. In particular, high optical absorption suggests a mixture of metallic TiH_2 particles in a dielectric MgH_2 matrix having a coherently integrated structure, as shown in Figure 1.[15,17]

Some indirect evidence for the presence of TiH_2 clusters in Mg-rich $Mg_xTi_{1-x}H_y$ thin films has been presented by extended X-ray absorption fine structure (EXAFS)[18] and positron annihilation[19] studies. Furthermore, theoretical calculations have shown that clustering of Ti atoms in Mg-rich thin films can effectively lower the mixing enthalpy per Ti atom.[20] Although these results support a chemically segregated but structurally coherent model for $Mg_xTi_{1-x}H_y$ thin films, direct

Received: January 7, 2020
Published: May 7, 2020

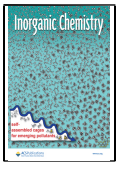

https://dx.doi.org/10.1021/acs.inorgchem.0c00059
Inorg. Chem. 2020, 59, 6800–6807

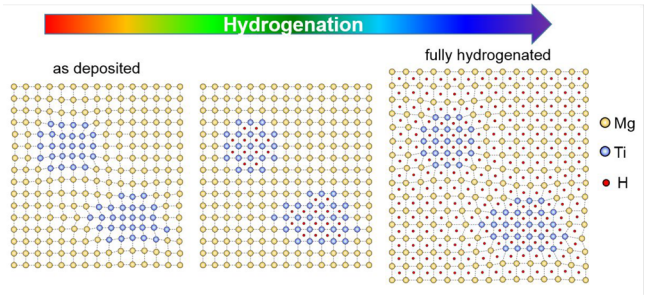

Figure 1. Schematic drawing of hydrogen uptake process of Mg-rich Mg_xTi_{1-x} thin films suggested in ref 15. In as-deposited thin films, Ti clusters are coherently embedded in a Mg matrix. On hydrogenation Ti clusters absorb hydrogen first and the Mg matrix absorbs hydrogen later.

experimental evidence for this unique structure and its details, such as the size and lattice expansion of the TiH_2-clusters, are still missing. This is mainly because the strong texture makes structure determination difficult.

The fact that conventional XRD perceives $Mg_xTi_{1-x}H_y$ thin films as solid solutions implies that chemical segregation occurs on a nanometer scale: the suggested TiH_2 clusters cannot be larger than a few nanometers. Identifying such small clusters coherently embedded in a matrix having a structure similar to that of the clusters is not straightforward and requires techniques that allow exploration of the atomic arrangement across multiple length scales. The PDF technique[21] is a powerful local structural probing technique that has been successfully applied to resolving nanoscale structural features in various materials.[22−24] The successful investigation of amorphous and crystalline $FeSb_3$ thin films using PDF was carried out by Jensen previously.[25] More recently, grazing-incidence X-ray diffraction has been successfully applied for the PDF study of Pt thin films.[26] However, we cannot utilize the same experimental setup for highly textured thin films.

In this work, we introduce a simple way of solving a preferred orientation problem to obtain X-ray PDFs of highly textured thin films. Our in situ PDFs of $Mg_{0.7}Ti_{0.3}$ thin films obtained during hydrogen absorption clearly show the presence of TiH_2 clusters with an average size of 30 Å embedded in a Mg matrix. During hydrogen uptake, the Mg matrix exhibits an intermediate face-centered-tetragonal (fct) phase that has not been reported before and the fully hydrogenated Mg matrix adopts an fcc structure imposed by the TiH_2 clusters. We also demonstrate how our PDF results and previous optical measurement results complement each other to reveal the extent of intermixing of immiscible Mg and Ti in TiH_2 clusters. This work demonstrates the great potential of the PDF technique for investigating nanoscale structural features in highly textured multicomponent thin films, which may be closely linked to their properties.

EXPERIMENTAL METHODS

PDF analysis is often performed on isotropic scattering data.[21] However, highly textured thin films usually yield only a few intense Bragg peaks, as shown in Figure S1c, and lead to PDFs with incomplete structural information (Figure S3a). This preferred orientation problem has been a major barrier to the PDF analysis of highly textured thin films. Although three-dimensional PDF analysis[27−29] is an ideal method for our study, it is experimentally more challenging and mathematically more complicated than PDF analysis of powder samples. In this study, we tried to obtain powder-diffraction-like data from thin films by adopting the following approach. We deposited a $Mg_{0.7}Ti_{0.3}$ thin film on a thin Kapton sheet, then cut it into small pieces, and packed the pieces in a Kapton capillary. A schematic overview of the experimental procedures is shown in Figure S2a. X-ray total scattering data obtained in this way display many Bragg peaks (Figure S2c), and the corresponding PDF clearly determines the hcp structural correlation of the thin film (Figure S3b). The shape of diffraction peaks measured in this way is virtually identical with that from an uncut film (Figure S4). This demonstrates that cutting the thin film has not altered the crystal morphology, microstructure, and crystalline defects of the sample significantly. We tried to obtain delaminated thin films for comparison but failed. Even scraping off the thin film from substrates was difficult. Therefore, we think that severe delamination of the thin films did not occur.

Two $Mg_{0.7}Ti_{0.3}$ thin films of 400 nm thickness were prepared. These thin films have different thicknesses of a Pd capping layer, i.e. 1.5 nm (designated by $Mg_{0.7}Ti_{0.3}$-1) and 2.5 nm (designated by $Mg_{0.7}Ti_{0.3}$-2) and provide different rates of hydrogen uptake. Since Ti clusters and the Mg matrix absorb hydrogen at different rates, $Mg_{0.7}Ti_{0.3}$-1 is better matched to the faster hydrogenation process of the Ti clusters and $Mg_{0.7}Ti_{0.3}$-2 is better matched to the slower hydrogenation process of the Mg matrix. By using these two thin films, structural changes in the Ti clusters and the Mg matrix during hydrogen absorption can be unambiguously resolved (see Sample Preparation in the Supporting Information for details).

Synchrotron X-ray total scattering experiments were conducted at the BL22XU beamline at SPring-8.[30] The thin films were cut into small pieces with various shapes (square or ribbonlike shapes in the size $\lesssim 5 \times 0.6$ mm^2) and loaded them in in situ gas loading cells.[31] Details of our in situ cells and in situ gas loading setup can be found in ref 31. All the data of the thin films were collected at 300 K using the rapid acquisition pair distribution function (RA-PDF) technique.[32] For the experiment on the $Mg_{0.7}Ti_{0.3}$-1 thin film (the $Mg_{0.7}Ti_{0.3}$-2 thin film), a large image plate detector, R-AXISV manufactured by Rigaku (an amorphous silicon detector manufactured by PerkinElmer) was mounted orthogonal to the incident X-ray beam of 70.430 keV (69.933 keV). The sample to detector distance was determined geometrically using diffraction profiles of a standard sample, CeO_2, measured at several different distances, and it was 300 mm. The in situ cell was spun for ±30° during data collection. For the $Mg_{0.7}Ti_{0.3}$-1 thin film, data were collected while 1 MPa of hydrogen gas was being applied. Each point of the data was collected for 60 s. For the $Mg_{0.7}Ti_{0.3}$-2 thin film, as soon as 0.2 MPa of hydrogen gas was applied, hydrogen absorption started and data were collected during the reaction. For each data set, 240 frames of 2 s image data were collected continuously.

Image data were first integrated to one-dimensional data using the WinPIP program, which is derived from the PIP program[33] and developed at BL22XU at Spring-8, and series of integrated data were summed. Using the program PDFgetX2[34] the signal from an empty cell was subtracted from the raw data, Compton scattering and Laue diffuse scattering corrections were made, and the X-ray PDFs were obtained. Q_{max} = 16 Å^{-1} was used. Real space modeling was carried out using the program PDFgui.[35] Basic information about PDF modeling is available in the Supporting Information.

RESULTS AND DISCUSSION

The low-2θ region of the X-ray total scattering data of the $Mg_{0.7}Ti_{0.3}$-2 thin film is shown in Figure 2. Before hydrogen uptake, three slightly broad but well distinct diffraction peaks corresponding to the (010), (002), and (011) reflections of an hcp structure are observed. The lattice parameters corresponding to these diffraction peaks are $a = b$ = 3.1041(9) Å and c = 4.989(2) Å, which are smaller than the lattice parameters of Mg ($a = b$ = 3.2085 Å and c = 5.2106 Å) but larger than those of Ti ($a = b$ = 2.95111 Å and c = 4.68433 Å).[36,37] As soon as hydrogen absorption begins, these three diffraction peaks

https://dx.doi.org/10.1021/acs.inorgchem.0c00059
Inorg. Chem. 2020, 59, 6800−6807

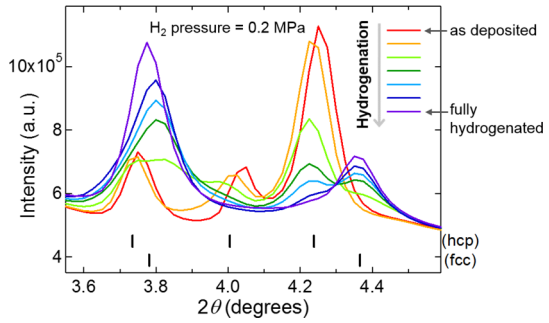

Figure 2. X-ray total scattering data of a $Mg_{0.7}Ti_{0.3}$-2 thin film collected during the hydrogenation process. Small vertical lines below the data indicate the positions of the (010), (002), and (011) reflections of an hcp structure and the positions of the (111) and (002) reflections of an fcc structure.

slightly shift to lower 2θ angles as if a hydrogen solid solution phase is formed, in which a small amount of hydrogen randomly occupies interstitial sites of the metal lattice. As hydrogen uptake proceeds further, the intensities of these diffraction peaks gradually decrease and concurrently new peaks emerge at $2\theta \approx 3.8$ and 4.37°. These new peaks can be assigned to the (111) and (002) reflections of an fcc structure, respectively, and continuously grow until the hcp reflections have completely disappeared. The lattice parameter of the fcc phase corresponding to the diffraction peaks of the fully hydrogenated sample is a = 4.616(1) Å, which is larger than the reported value for bulk TiH_2 (a = 4.4512 Å).[38]

Both bulk magnesium and titanium crystallize in the hcp structure (space group $P6_3/mmc$). On hydrogenation they transform into MgH_2 with a rutile-type tetragonal structure (space group $P4_2/mnm$) and TiH_2 with a fluorite-type fcc structure (space group $Fm\bar{3}m$), respectively.[39] This is a first-order phase transformation, and hence, a hydrogen solid solution phase (e.g., MgH_δ or TiH_δ) and a hydride phase (e.g., MgH_2 or TiH_2) coexist in the system during transition. The diffraction patterns shown in Figure 2 suggest that the hydrogenation process of the $Mg_{0.7}Ti_{0.3}$ thin film is comparable to that of bulk Ti: a hydrogen solid solution phase having an hcp structure transforms into a hydride phase having an fcc structure via a mixed-phase regime. This is in accord with previous X-ray and TEM study results. Changes in diffraction peaks remind us of nothing but a solid solution alloy thin film and do not give any clues to chemical segregation.

Figure 3 shows the PDFs obtained during hydrogenation of the $Mg_{0.7}Ti_{0.3}$-1 thin film. Before hydrogenation, a single hcp model (a $Mg_{0.7}Ti_{0.3}$ solid solution model) is sufficient to explain the experimental PDF over a wide r range, 1.5 < r < 80 Å (Figure 3a). The refined lattice parameters are $a = b$ = 3.115(1) Å and c = 5.005(3) Å. These are smaller than the lattice parameters of Mg ($a = b$ = 3.2085 Å and c = 5.2106 Å) but larger than those of Ti ($a = b$ = 2.95111 Å and c = 4.68433 Å).[36,37] Interestingly, these values are rather close to the calculated values for a $Mg_{0.7}Ti_{0.3}$ solid solution alloy ($a = b$ = 3.1313 Å and c = 5.0527 Å) using Vegard's law.[40] This good fit is obtained at the expense of a large isotropic atomic displacement parameter (U_{iso} = 0.041(7) Å^2), indicating the presence of large random displacement in the sample.[41] We also tried two-phase modeling using a nanosized hcp Ti model and an hcp Mg model. However, the fit did not improve despite a greater number of parameters being used. Moreover, the refined U_{iso} value for Ti was very large ($U_{iso} \sim 0.4$ Å^2). As

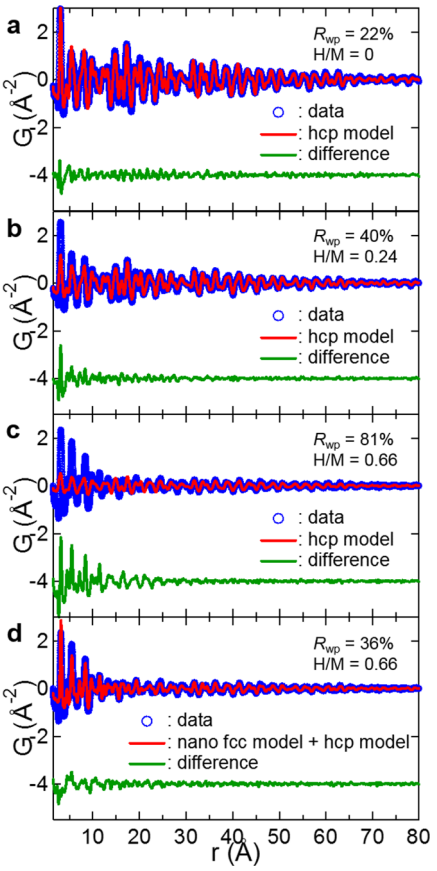

Figure 3. PDFs of the $Mg_{0.7}Ti_{0.3}$-1 thin film obtained during hydrogen absorption. The experimental PDFs of (a) the as-deposited thin film and (b, c) the thin film during hydrogenation are compared with the calculated PDFs of refined hcp $Mg_{0.7}Ti_{0.3}$ structure models. The difference between the measured and the calculated PDFs is presented by the lower green line. (d) Two-phase fit to the experimental PDF shown in (c) using an fcc TiH_2 nanoparticle model and an hcp Mg model. The PDF in (c) and (d) is the state in which hydrogenation of Ti clusters is completed. The amount of absorbed hydrogen (H/M = the number ratio of hydrogen to metal atoms) is estimated from the refined phase fraction of TiH_2. R_{wp} is the goodness of fit. The R_{wp} value of (a) is comparable to those obtained from $FeSb_3$ thin films in ref 25.

we mentioned earlier, the as-deposited thin film is largely disordered and this makes detailed PDF features indistinct. Consequently, it is difficult to distinguish two hcp structures having similar lattice parameters from the low-r region of the PDF. Therefore, no clear hint of chemical segregation is found in this PDF.

When 1 MPa of hydrogen gas is applied, the film first slightly expands its volume but keeps the hcp structure. The lattice parameters increase to $a = b$ = 3.130(2) Å and c = 5.051(1) Å (Figure S5). This indicates the formation of a hydrogen solid solution phase. The fit in this case is as good as in the as-deposited case, and the refined U_{iso} value decreases slightly to 0.038(3) Å^2. As hydrogenation proceeds further, new features arise in the PDF (Figure 3b). These features only appear at $r \lesssim$ 30 Å and continuously grow (Figure 3c). In contrast, the high-r region ($r \gtrsim$ 30 Å) remains unchanged. Modeling these data reveals that new intensities are due to the formation of a fluorite-type fcc phase. As shown in Figure 3d, a significantly improved fit is obtained by combining an hcp Mg model and a fluorite-type fcc TiH_2 nanoparticle model. The atomic ratio of

https://dx.doi.org/10.1021/acs.inorgchem.0c00059
Inorg. Chem. 2020, 59, 6800−6807

Mg to Ti obtained from PDF refinement is 0.67:0.33, close to the target composition. This PDF result unambiguously reveals that the $Mg_{0.7}Ti_{0.3}$ thin film at this stage consists of Ti-rich regions with an average size of 30 Å (TiH_2 clusters) and Mg-rich regions with a structural coherence length larger than 80 Å (a Mg matrix). The result is more or less consistent with the chemical segregation picture proposed in ref 15 (Figure 1). Although two-phase modeling provides a fairly good fit, broad fluctuations in the low-r region of the difference curve (Figure 3d) indicate that some PDF features are still not explained. These features are most likely from the interface between fcc TiH_2 clusters and the hcp Mg matrix. The refined lattice parameter for the TiH_2 nanoparticle model is a = 4.516(9) Å. The value is larger than the reported value for bulk TiH_2 (a = 4.4512 Å)[38] probably due to the presence of some larger Mg atoms inside TiH_2 clusters or the coherent clamping of TiH_2 clusters with the Mg matrix. We will discuss about this point in detail later. A spherical nanoparticle model was used to explain the TiH_2 clusters, and the particle size fluctuates with the PDF profile parameters around 30 Å (between 25 and 36 Å). This is probably because the clusters do not have a spherical shape.

To investigate structural change in the Mg matrix on hydrogenation, we analyzed the PDF data obtained from the $Mg_{0.7}Ti_{0.3}$-2 thin film. We focus on change in the 30 < r < 80 Å region, where the contribution of the Mg matrix is predominant. As shown in Figure 4a, the as-deposited $Mg_{0.7}Ti_{0.3}$ thin film exhibits sharp PDF peaks representing an hcp structure. This indicates the presence of well-defined structural correlation over a long distance. Lattice parameters obtained by fitting the 30 < r < 80 Å region are a = b = 3.130(1) Å and c = 5.031(5) Å. These are slightly larger than the values obtained from the $Mg_{0.7}Ti_{0.3}$-1 thin film. At a point 600 s after the introduction of 0.2 MPa of hydrogen gas, a hydrogen solid solution phase with lattice parameters of a = b = 3.142(6) Å and c = 5.070(3) Å is formed. Hydrogenation progresses steadily. The experimental PDF shown in Figure 4b represents the state where most of the Ti clusters are transformed to the fcc hydride phase. The low-r region of this PDF is well explained by a nanosized fcc TiH_2 model and an hcp Mg model as shown in Figure S6. Although a small variation in peak intensity is seen in Figure 4b, the hcp structural features in this region remain intact. The lattice parameters become slightly larger than those of the hydrogen solid solution phase (δa = δb = 0.008 Å, δc = 0.018 Å; see Table S1) probably due to the hydrogenation of the Ti clusters and the resulting lattice expansion thereof. Unaltered PDF features at r > 30 Å and a subtle change in the lattice parameters of the hcp matrix at this stage suggest the possibility of pre-existing Ti clusters in the as-deposited thin films. If TiH_2 clusters were formed from a Mg−Ti random alloy by hydrogenation, we would have seen a much larger change in the lattice parameters of the hcp matrix due to the occurrence of chemical segregation (alloying of Mg with 30 atom % of Ti will lead to changes in lattice parameters by $\delta a \approx -0.077$ Å and $\delta c \approx -0.158$ Å). The fit shown in Figure S6 yields an atomic ratio of Mg to Ti of 0.71:0.29. This thin film is slightly richer in Mg than the other film.

After the hydrogenation of Ti clusters is completed (3000 s after hydrogen introduction), fluorite-type fcc structural features start to emerge at r > 30 Å (Figure 4c). Since there is a long interval of time between the advent of fcc signals in this region and in the region of r < 30 Å (1260 s), we attribute this change to the metal hydride transformation of the Mg

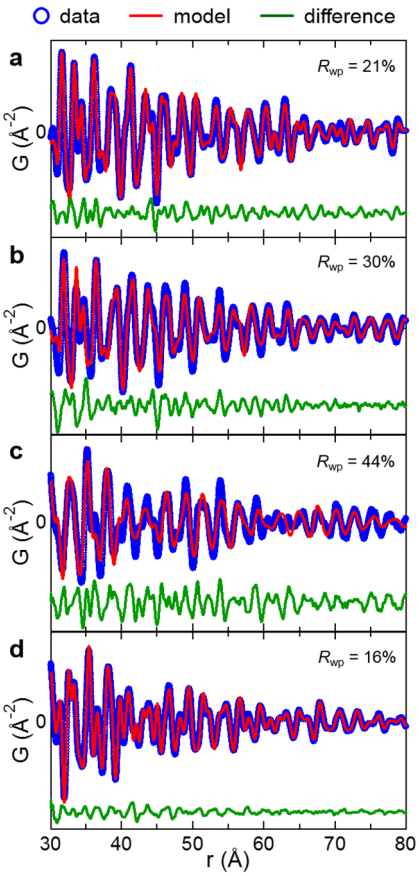

Figure 4. 30 < r < 80 Å region of the PDFs of $Mg_{0.7}Ti_{0.3}$-2 thin film. Experimental PDFs of (a) the as-deposited thin film and (b) the complete hydrogenation state of Ti clusters are shown and an hcp Mg model is fit to the data. (c) One of the PDFs obtained during the hydrogenation of the Mg matrix is shown. An fcc MgH_2 model is used to fit the PDF. (d) PDF of the complete hydrogenation state of the Mg matrix. A single fcc MgH_2 model explains all the PDF features.

matrix. During this transition, the 30 < r < 80 Å region should be explained by a combination of two structure models: i.e. an hcp structure model for the metal part and a fluorite-type fcc structure model for the hydride part. However, such two-phase modeling provides an imperfect fit (Figure 5a); in particular, features at r > 57 Å are poorly reproduced. It turns out that to fully understand structural changes in this region an fct model, which is close to the fluorite-type fcc structure but whose one cell axis is slightly shorter than the others, is necessary. Figure 5b shows the result of three-phase modeling. Now, all the PDF features at r > 57 Å are well reproduced and even the r < 57 Å region is explained better. None of the combinations of any two models yield such a good fit. The refined structural parameters are given in Table S2. Note that we did not see the formation of the fcc and fct MgH_2 phases in $Mg_{0.7}Ti_{0.3}$-1 thin film because its hydrogen uptake rate is too slow to detect the slower hydrogenation process of the Mg matrix during the experiment.

Hydrogen absorption by the thin film slows down as the metal to hydride transformation of the Mg matrix progresses. After nearly 90% of the Mg matrix underwent transformation, only a very subtle change occurred in the PDF over time. One of the possible reasons for a decrease in hydrogenation rate of the Mg matrix is discussed in the Supporting Information. To

https://dx.doi.org/10.1021/acs.inorgchem.0c00059
Inorg. Chem. 2020, 59, 6800−6807

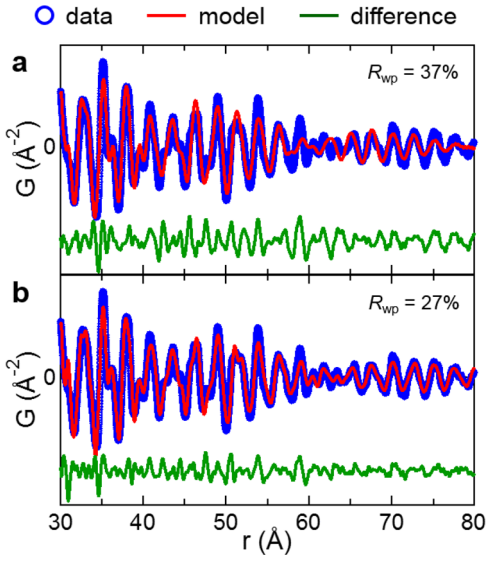

Figure 5. Experimental PDF of $Mg_{0.7}Ti_{0.3}$-2 thin film shown in Figure 4c. (a) An hcp Mg model and an fcc MgH_2 model (two-phase modeling) and (b) an hcp Mg model, an fcc MgH_2 model, and an fct MgH_2 model (three-phase modeling) were fit to the experimental PDF.

accelerate the reaction, the sample was heated at 373 K for 120 s under a hydrogen gas environment. After heating, it reached the state of complete hydrogenation. A single fluorite-type fcc structural model yields an excellent fit (Figure 4d), indicating that the Mg matrix completely transforms to the fcc hydride phase. An excellent two-phase fitting result using an fcc TiH_2 nanoparticle model and an fcc MgH_2 model over a wider r range, $1.5 < r < 80$ Å, is shown in Figure S7.

The Mg matrix exhibits two interesting characteristics. First, while bulk Mg forms a rutile-type tetragonal hydride, the Mg matrix of the $Mg_{0.7}Ti_{0.3}$ thin film forms a fluorite-type fcc hydride. There are two reported Mg-based hydrides having a fluorite-type fcc metal sublattice. One of these is a high-pressure polymorph of MgH_2 having a modified fluorite structure (space group $Pa\bar{3}$).[42,43] Interestingly, its lattice constant (a = 4.6655 Å) is close to that of our fully hydrogenated Mg matrix (a = 4.658 Å). The other known hydride is $Mg_7TiH_{12.7}$. In this phase, Mg is arrayed in a doubled TiH_2 unit cell and Ti atoms occupy the 4a site (Ga_7Ge-type structure, a = 9.532 Å).[44] At present, it is not clear whether the fully hydrogenated Mg matrix forms either of these hydride phases, but it is apparent that it does not take a rutile-type tetragonal structure. Then, what causes the formation of an fcc MgH_2 matrix? We may think of reduced dimensionality or clamping effect from the substrate as a possible cause. However, our unpublished PDF study shows that a Ti-free MgH_2 thin film of 400 nm thickness takes a rutile-type tetragonal structure. Indeed, fcc MgH_2 is observed in $Mg_xTi_{1-x}H_y$ thin films for only $x < 0.85$[15,45] and is not found in Mg−Ti−H multilayer thin films.[46,47] All of these indicate that nanosized Ti clusters (or TiH_2 clusters) play an important role and they strongly interact with the Mg matrix. In other words, they are structurally integrated as suggested in ref 15 (Figure 1). A change in the PDF peak widths of the Mg matrix during hydrogenation also hints at the structural integration (see the Supporting Information).

The other interesting characteristic of the Mg matrix is the emergence of an fct MgH_2 phase during transition. This phase was not reported previously. None of the known high-pressure polymorphs of MgH_2 take an fct structure. Figure 6a shows

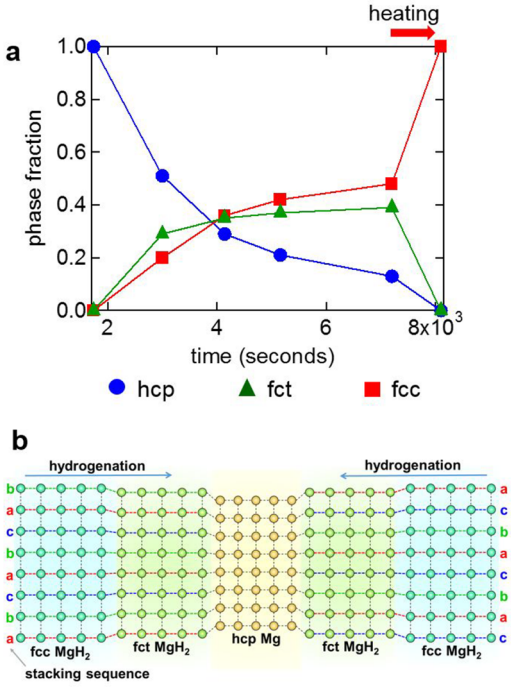

Figure 6. (a) Phase fraction of hcp Mg, fct MgH_2, and fcc MgH_2 during hydrogenation of the Mg matrix are plotted as a function of reaction time. (b) A schematic diagram of the development of fct MgH_2 and fcc MgH_2 is shown.

how the phase fraction of hcp Mg, fct MgH_2, and fcc MgH_2 varies during hydrogen uptake by the Mg matrix. The fct phase appears concurrently with the fcc MgH_2 phase. The development of these two phases is very rapid at the beginning but gradually slows down after more than 66% of the Mg matrix transforms into either of these phases. Their phase fractions are comparable to each other throughout the transition, but at the end of the transition the fct phase disappears with the hcp phase. It appears that fct MgH_2 can be present only when fcc MgH_2 and hcp Mg coexist.

The hcp−fcc phase transformation is observed in numerous materials,[48−53] and there are a few cases where an intermediate phase (or an intermediate structure) having characteristics similar to those of our fct MgH_2 phase is seen.[52,53] This intermediate structure is formed at the interface between the hcp and the fcc structures to decrease the distortion energy caused by a lattice mismatch and disappears when the transition is completed. A similar intermediate phase is also found in $LiFePO_4$ during nonequilibrium battery operation to reduce a lattice mismatch between $LiFePO_4$ and $FePO_4$ and to promote a fast phase transition.[54]

The X-ray diffraction pattern of an as-deposited $Mg_{0.7}Ti_{0.3}$ thin film measured in reflection geometry shows only the (002) reflection of an hcp structure.[15] After hydrogenation, the (111) reflection of an fcc structure is seen. It can be easily deduced that the hcp to fcc structural change occurs via the conversion of (002) planes of the hcp structure into (111) planes of the fcc structure. The interplanar distance of (002) planes of hcp Mg and that of (111) planes of fcc MgH_2 obtained from the refined lattice parameters in Table S2 are 2.549 and 2.697 Å, respectively. The interplanar spacing of

https://dx.doi.org/10.1021/acs.inorgchem.0c00059
Inorg. Chem. 2020, 59, 6800−6807

(111) planes of fct MgH_2 is 2.659 Å. Thus, it is most likely that fct MgH_2 is formed between hcp Mg and fcc MgH_2 to reduce distortion energy caused by a lattice mismatch between them (Figure 6b). Note that the interplanar spacing of (111) planes of fcc TiH_2 is 2.642 Å, comparable to that of fct MgH_2. The presence of the fct MgH_2 phase probably prevents $Mg_{0.7}Ti_{0.3}$ thin films from pulverization that often occurs during hydrogenation of bulk materials owing to large volume expansion. Therefore, it allows these metastable thin films to retain their structure over several hydrogenation and dehydrogenation cycles and promotes fast hydrogen uptake.[45]

Finally, we utilize the optical transmission measurement results in ref 17 to explain the lattice parameter of the TiH_2 clusters. Gremaud et al. measured pressure−optical−transmission isotherms of $Mg_xTi_{1-x}H_y$ thin films by using hydrogenography[55] and extracted the values for the chemical short-range order parameter (s) and the parameter related to the degree of local deformation of a cluster embedded in an alloy (L). Details of these parameters can be found in ref 17. From their optical analysis Gremaud et al. obtained s = 0.34 and L = 0.2 for a $Mg_{0.7}Ti_{0.3}$ thin film. They could not determine a cluster size. Our PDF analysis showed that the average size of the TiH_2 clusters in the hydrogenated $Mg_{0.7}Ti_{0.3}$-2 thin film is ∼30 Å. For a 30 Å TiH_2 cluster embedded in a Mg matrix to have s = 0.34, approximately 17% of the constituent atoms should be Mg (see the Supporting Information for details). By simply adopting Vegard's law with the lattice parameters of bulk TiH_2 (a = 4.4512 Å) and the high-pressure phase of MgH_2 having a modified fluorite structure (a = 4.6655 Å), we obtain a = 4.4876 Å for $Mg_{0.17}Ti_{0.83}H_2$. This value is still smaller than the lattice parameter of the TiH_2 clusters obtained from PDF analysis, a = 4.572 Å. If we consider the local deformation of the cluster due to coherent embedment in an alloy matrix as mentioned in ref 17, the lattice parameter of our model becomes 4.5784 Å. This is very close to the value obtained from PDF analysis. This shows that the PDF results are essentially consistent with optical measurement results and additional information such as the average chemical composition of TiH_2 clusters, which is $Mg_{0.17}Ti_{0.83}H_y$, can be extracted. More importantly, this result sheds light on how compositional modulation occurs in metastable thin films created between immiscible elements.

CONCLUSIONS

In conclusion, the structural evolution of highly textured $Mg_{0.7}Ti_{0.3}$ thin films during hydrogenation was investigated by using PDF analysis. Our study clarifies the presence of TiH_2 clusters of an average size of ∼30 Å and confirms previous findings that the hydrogenated Mg matrix takes an fcc structure. During hydrogenation of the Mg matrix a previously unknown MgH_2 intermediate phase having an fct structure was observed. This intermediate phase is probably important for the structural stability of this metastable thin film during hydrogen uptake. We also showed how PDF and optical measurement results complement each other to provide information on the average composition of TiH_2 clusters and a better picture of how compositional modulation occurs in this system. Our method can be applied to a wide variety of thin films to resolve nanoscale compositional and structural heterogeneities, which are closely linked to their fascinating properties, and the structural response of each constituent part during various physical and chemical reactions.

ASSOCIATED CONTENT

Supporting Information

The Supporting Information is available free of charge at https://pubs.acs.org/doi/10.1021/acs.inorgchem.0c00059.

Comparison of data obtained using two different setups, sample preparation, PDF fitting results, refined structural parameters, and calculations for the lattice parameter of TiH_2 clusters (PDF)

AUTHOR INFORMATION

Corresponding Author

Hyunjeong Kim − *National Institute of Advanced Industrial Science and Technology, Tsukuba, Ibaraki 305-8569, Japan;* orcid.org/0000-0001-5018-3173; Phone: +81 29 861 0551; Email: hj.kim@aist.go.jp

Authors

Herman Schreuders − *Department of Chemical Engineering, MECS, Delft University of Technology, 2629 HZ Delft, The Netherlands*

Kouji Sakaki − *National Institute of Advanced Industrial Science and Technology, Tsukuba, Ibaraki 305-8569, Japan;* orcid.org/0000-0003-4781-1073

Kohta Asano − *National Institute of Advanced Industrial Science and Technology, Tsukuba, Ibaraki 305-8569, Japan;* orcid.org/0000-0003-4208-7303

Yumiko Nakamura − *National Institute of Advanced Industrial Science and Technology, Tsukuba, Ibaraki 305-8569, Japan*

Naoyuki Maejima − *Department of Chemistry, Rikkyo University, Tokyo 171-8501, Japan*

Akihiko Machida − *National Institutes for Quantum and Radiological Science and Technology, Sayo, Hyogo 679-5148, Japan*

Tetsu Watanuki − *National Institutes for Quantum and Radiological Science and Technology, Sayo, Hyogo 679-5148, Japan*

Bernard Dam − *Department of Chemical Engineering, MECS, Delft University of Technology, 2629 HZ Delft, The Netherlands;* orcid.org/0000-0002-8584-7336

Complete contact information is available at: https://pubs.acs.org/10.1021/acs.inorgchem.0c00059

Notes

The authors declare no competing financial interest.

ACKNOWLEDGMENTS

This work was partially supported by Photon and Quantum Basic Research Coordinated Development Program from the Ministry of Education, Culture, Sports, Science and Technology (MEXT) of Japan and by the International Joint Research Program for Innovative Energy Technology by the Ministry of Economy, Trade and Industry (METI) of Japan. The synchrotron X-ray experiments were performed using the QST experimental station at the JAEA beamlines of BL22XU (Proposal No. 2013B3783, No. 2014B3703, No. 2014B3784, No. 2015A3703, No. 2015A3784, No. 2016A3753, and No. 2016A3788) at SPring-8 under the Shared Use Program of JAEA and QST Facilities (Proposal No. 2013B-E21, No. 2014B-E20, No. 2015A-E17, and No. 2016A-E23). The use of the JAEA beamline of BL22XU is also supported by the JAEA and QST Advanced Characterization Nanotechnology Platform under remit of "Nanotechnology Platform" of MEXT of

Japan under Proposal No. A-13-AE-0038, No. A-14-AE-0042, No. A-15-AE-0017, and No. A-16-QS-0015.

REFERENCES

(1) Venkatasubramanian, R.; Siivola, E.; Colpitts, T.; O'Quinn, B. Thin-film thermoelectric devices with high room-temperature figures of merit. *Nature* **2001**, *413*, 597−602.

(2) Huiberts, J. N.; Griessen, R.; Rector, J. H.; Wijngaarden, R. J.; Dekker, J. P.; de Groot, D. G.; Koeman, N. J. Yttrium and lanthanum hydride films with switchable optical properties. *Nature* **1996**, *380*, 231−234.

(3) Kirtley, J. R.; Tsuei, C. C.; Sun, J. Z.; Chi, C. C.; Yu Jahnes, L. S.; Gupta, A.; Rupp, M.; Ketchen, M. B. Symmetry of the ordr parameter in the high-T_c superconductor $YBa_2Cu_3O_{7-\delta}$. *Nature* **1995**, *373*, 225−228.

(4) Ma, E. Alloys created between immiscible elements. *Prog. Mater. Sci.* **2005**, *50*, 413−509.

(5) Fortunato, E.; Barquinha, P.; Martins, R. Oxide Semiconductor Thin-Film Transistors: A Review of Recent Advances. *Adv. Mater.* **2012**, *24*, 2945−2986.

(6) Setter, N.; Damjanovic, D.; Eng, L.; Fox, G.; Gevorgian, S.; Hong, S.; Kingon, A.; Kohlstedt, H.; Park, N. Y.; Stephenson, G. B.; Stolitchnov, I.; Taganstev, A. K.; Taylor, D. V.; Yamada, T.; Streiffer, S. Ferroelectric thin films: Review of materials, properties, and applications. *J. Appl. Phys.* **2006**, *100*, 051606.

(7) Pulker, H. K. Characterization of optical thin films. *Appl. Opt.* **1979**, *18*, 1969−1977.

(8) Shah, A.; Torres, P.; Tscharner, R.; Wyrsch, N.; Keppner, H. Photovoltaic Technology: The Case for Thin-Film Solar Cells. *Science* **1999**, *285*, 692−698.

(9) Hemminger, J. C.; Sarrao, J.; Crabtree, G.; Flemming, G.; Ratner, M. *Challenges at the Frontiers of Matter and Energy: Transformative Opportunities for Discovery Science*; U.S. Department of Energy Office of Science: 2015. DOI: 10.2172/1283188.

(10) Holder, A. M.; Siol, S.; Ndione, P. F.; Peng, H.; Deml, A. M.; Matthews, B. E.; Schelhas, L. T.; Toney, M. F.; Gordon, R. G.; Tumas, W.; et al. Novel phase diagram behavior and materials design in heterostructural semiconductor alloys. *Sci. Adv.* **2017**, *3*, No. e1700270.

(11) Niessen, R. A. H.; Notten, P. H. L. Electrochemical Hydrogen Storage Characteristics of Thin Film MgX (X = Sc, Ti, V, Cr) Compounds. *Electrochem. Solid-State Lett.* **2005**, *8*, A534−A538.

(12) Borsa, D. M.; Baldi, A.; Pasturel, M.; Schreuders, H.; Dam, B.; Griessen, R.; Vermeulen, P.; Notten, P. H. L. Mg-Ti-H thin films for smart solar collectors. *Appl. Phys. Lett.* **2006**, *88*, 241910.

(13) Baldi, A.; Borsa, D. M.; Schreuders, H.; Rector, J. H.; Atmakidis, T.; Bakker, M.; Zondag, H. A.; van Helden, W. G. J.; Dam, B.; Griessen, R. Mg-Ti-H thin films as switchable solar absorbers. *Int. J. Hydrogen Energy* **2008**, *33*, 3188−3192.

(14) Slaman, M.; Dam, B.; Schreuders, H.; Griessen, R. Optimization of Mg-based fiber optic hydrogen detectors by alloying the catalyst. *Int. J. Hydrogen Energy* **2008**, *33*, 1084−1089.

(15) Borsa, D. M.; Gremaud, R.; Baldi, A.; Schreuders, H.; Rector, J. H.; Kooi, B.; Vermeulen, P.; Notten, P. H. L.; Dam, B.; Griessen, R. Structural, optical, and electrical properties of $Mg_yTi_{1-y}H_x$ thin films. *Phys. Rev. B: Condens. Matter Mater. Phys.* **2007**, *75*, 205408.

(16) Murray, J. L. *Phase Diagrams of Binary Titanium Alloys*; ASM International: 1990.

(17) Gremaud, R.; Baldi, A.; Gonzalez-Silveira, M.; Dam, B.; Griessen, R. Chemical short-range order and lattice deformations in $Mg_yTi_{1-y}H_x$ thin films probed by hydrogenography. *Phys. Rev. B: Condens. Matter Mater. Phys.* **2008**, *77*, 144204.

(18) Baldi, A.; Gremaud, R.; Borsa, D. M.; Baldé, C. P.; van der Eerden, A. M. J.; Kruijtzer, G. L.; de Jongh, P. E.; Dam, B.; Griessen, R. Nanoscale composition modulations in $Mg_yTi_{1-y}H_x$ thin film alloys for hydrogen storage. *Int. J. Hydrogen Energy* **2009**, *34*, 1450−1457.

(19) Leegwater, H.; Schut, H.; Egger, W.; Baldi, A.; Dam, B.; Eijt, S. W. H. Divacancies and the hydrogenation of Mg-Ti films with short range chemical order. *Appl. Phys. Lett.* **2010**, *96*, 121902.

(20) Jensen, I. J. T.; Diplas, S.; Løvvik, O. M. Density functional calculations of Ti nanoclusters in the metastable Mg-Ti system. *Phys. Rev. B: Condens. Matter Mater. Phys.* **2010**, *82*, 174121.

(21) Egami, T.; Billinge, S. J. L. *Underneath the Bragg Peaks: Structural Analysis of Complex Materials*; Pergamon Press Elsevier: Oxford, England, 2003.

(22) Billinge, S. J. L.; Kanatzidis, M. G. Beyond crystallography: the study of disorder, nanocrystallinity and crystallographically challenged materials with pair distribution functions. *Chem. Commun.* **2004**, *7*, 749−760.

(23) Proffen, Th.; Kim, H. Advances in total scattering analysis. *J. Mater. Chem.* **2009**, *19*, 5078−5088.

(24) Young, C. A.; Goodwin, A. L. Applications of pair distribution function methods to contemporary problems in materials chemistry. *J. Mater. Chem.* **2011**, *21*, 6464−6476.

(25) Jensen, K. M. Ø.; Blichfeld, A. B.; Bauers, S. R.; Wood, S. R.; Dooryhée, E.; Johnson, D. C.; Iversen, B. B.; Billinge, S. J. L. Demonstration of thin film pair distribution function analysis (tfPDF) for the study of local structure in amorphous and crystalline thin films. *IUCrJ* **2015**, *2*, 481−489.

(26) Roelsgaard, M.; Dippel, A. C.; Borup, K. A.; Nielsen, I. G.; Broge, N. L. N.; Roh, J. T.; Gutowski, O.; Iversen, B. B. Time-resolved grazing-incidence pair distribution functions during deposition by raaio-frequency magnetron sputtering. *IUCrJ* **2019**, *6*, 299−304.

(27) Schaub, P.; Weber, T.; Steurer, W. Analysis and modeling of structural disorder by the use of the three-dimensional pair distribution function method exemplified by the disordered twofold superstructure of decagonal Al-Cu-Co. *J. Appl. Crystallogr.* **2011**, *44*, 134−149.

(28) Weber, T.; Simonov, A. The three-dimensional pair distribution function analysis of disordered single crystals: basic concepts. *Z. Kristallogr.* **2012**, *227*, 238−247.

(29) Simonov, A.; Weber, T.; Steurer, W. Experimental uncertainties of three-dimensional pair distribution function investigations exemplified on the diffuse scattering from a tris-*tert*-butyl-1, 3, 5-benzene tricarboxamide single crystal. *J. Appl. Crystallogr.* **2014**, *47*, 2011−2018.

(30) Watanuki, T.; Machida, A.; Ikeda, T.; Ohmura, A.; Kaneko, H.; Aoki, K.; Sato, T. J.; Tsai, A. P. Development of a Single-Crystal X-ray Diffraction System for Hydrostatic-Pressure and Low-Temperature Structural Measurement and Its Application to the Phase Study of Quasicrystals. *Philos. Mag.* **2007**, *87*, 2905−2911.

(31) Sakaki, K.; Kim, H.; Machida, A.; Watanuki, T.; Katayama, Y.; Nakamura, Y. Development of an in situ synchrotron X-ray total scattering setup under pressurized hydrogen gas. *J. Appl. Crystallogr.* **2018**, *51*, 796−801.

(32) Chupas, P. J.; Qiu, X.; Hanson, J. C.; Lee, P. L.; Grey, C. P.; Billinge, S. J. L. J. Rapid-Acquisition Pair Distribution Function (RA-PDF) Analysis. *J. Appl. Crystallogr.* **2003**, *36*, 1342−1347.

(33) Fujihisa, H. An X-ray Powder Pattern Analysis Program for Imaging Plate. *Koatsuryoku no Kagaku to Gijutsu* **1999**, *9*, 65−70.

(34) Qiu, X.; Thompson, J. W.; Billinge, S. J. L. PDFgetX2: A GUI Driven Program to Obtain the Pair Distribution Function from X-ray Powder Diffraction Data. *J. Appl. Crystallogr.* **2004**, *37*, 678.

(35) Farrow, C. L.; Juhas, P.; Liu, J. W.; Bryndin, D.; Božin, E. S.; Bloch, J.; Proffen, Th.; Billinge, S. J. L. PDFfit2 and PDFgui: Computer Programs for Studying Nanostructure in Crystals. *J. Phys.: Condens. Matter* **2007**, *19*, 335219.

(36) Owen, E. A.; Pickup, L.; Roberts, I. O. Lattice Constants of five Elements possessing Hexagonal Structure. *Z. Kristallogr. - Cryst. Mater.* **1935**, *91*, 70−76.

(37) Wood, R. M. The Lattice Constants of High Purity Alpha Titanium. *Proc. Phys. Soc., London* **1962**, *80*, 783−786.

(38) Kalita, P. E.; Sinogeikin, S. V.; Lipinska-Kalita, K.; Martmann, T.; Ke, X.; Chen, C.; Cornelius, A. Equation of state of TiH_2 up to 90 GPa: A synchrotron x-ray diffraction study and *ab initio* calculations. *J. Appl. Phys.* **2010**, *108*, 043511.

(39) Manchester, F. D. *Phase Diagrams of Binary Hydrogen Alloys*; ASM International: 2000.

https://dx.doi.org/10.1021/acs.inorgchem.0c00059
Inorg. Chem. 2020, 59, 6800−6807

(40) Vegard, L. Die konstitution der mischkristalle und die raumfüllung der atome. *Eur. Phys. J. A* **1921**, *5*, 17−26.
(41) Petkov, V.; Jeong, I.-K.; Chung, J. S.; Thorpe, M. F.; Kycia, S.; Billinge, S. J. L. High Real-Space Resolution Measurement of the Local Structure of $Ga_{1-x}In_xAs$ Using X-Ray Diffraction. *Phys. Rev. Lett.* **1999**, *83*, 4089−4092.
(42) Vajeeston, P.; Ravindran, P.; Kjekshus, A.; Fjellvåg, H. Pressure-Induced Structural Transitions in MgH_2. *Phys. Rev. Lett.* **2002**, *89*, 175506.
(43) Vajeeston, P.; Ravindran, P.; Hauback, B. C.; Fjellvåg, H.; Kjekshus, A.; Furuseth, S.; Hanfland, M. Structural stability and pressure-induced phase transitions in MgH_2. *Phys. Rev. B: Condens. Matter Mater. Phys.* **2006**, *73*, 224102.
(44) Kyoi, D.; Sato, T.; Rönnebro, E.; Kitamura, N.; Ueda, A.; Ito, M.; Katsuyama, S.; Hara, S.; Noréus, D.; Saki, T. A new ternary magnesium-titanium hydride Mg_7TiH_x with hydrogen desorption properties better than both binary magnesium and titanium hydrides. *J. Alloys Compd.* **2004**, *372*, 213−217.
(45) Vermeulen, P.; Wondergem, H. J.; Graat, P. C. J.; Borsa, D. M.; Schreuders, H.; Dam, B.; Griessen, R.; Notten, P. H. L. In situ electrochemical XRD study of (de)hydrogenation of Mg_yTi_{100-y} thin films. *J. Mater. Chem.* **2008**, *18*, 3680−3687.
(46) Baldi, A.; Pálsson, G. K.; Gonzales-Silveira, M.; Schreuders, H.; Slaman, M.; Rector, J. H.; Krishnan, G.; Kooi, B. J.; Walker, G. S.; Fay, M. W.; Hjörvarsson, B.; Wijngaarden, R. J.; Dam, B.; Griessen, R. Mg/Ti multilayers: Structural and hydrogen absorption properties. *Phys. Rev. B: Condens. Matter Mater. Phys.* **2010**, *81*, 224203.
(47) Mooij, L. P. A.; Baldi, A.; Boelsma, C.; Shen, K.; Wagemaker, M.; Pivak, Y.; Schreuders, H.; Griessen, R.; Dam, B. Interface Energy Controlled Thermodynamics of Nanoscale Metal Hydrides. *Adv. Energy Mater.* **2011**, *1*, 754−758.
(48) Yang, J. X.; Zhao, H. L.; Gong, H. R.; Song, M.; Ren, Q. Q. Proposed mechanism of HCP → FCC phase transition in titanium through first principles calculation and experiments. *Sci. Rep.* **2018**, *8*, 1992.
(49) Zhao, H.; Song, M.; Ni, S.; Shao, S.; Wang, J.; Liao, X. Atomic-scale understanding of stress-induced phase transformation in cold-rolled Hf. *Acta Mater.* **2017**, *131*, 271−279.
(50) Machida, A.; Ohmura, A.; Watanuki, T.; Ikeda, T.; Aoki, K.; Nakano, S.; Takemura, K. X-ray diffraction investigation of the hexagonal-fcc structural transition in yttrium trihydride under hydrostatic pressure. *Solid State Commun.* **2006**, *138*, 436−440.
(51) Machida, A.; Ohmura, A.; Watanuki, T.; Aoki, K.; Takemura, K. Long-period stacking structures in yttrium trihydride at high pressure. *Phys. Rev. B: Condens. Matter Mater. Phys.* **2007**, *76*, 052101.
(52) Blaschko, O.; Krexner, G.; Pleschiutschnig, J.; Ernst, G.; Hitzenberger, C.; Karnthaler, H. P.; Korner, A. Coherent Modulated Structure during the Martensitic hcp-fcc Phase Transition in Co and in a CoNi Alloy. *Phys. Rev. Lett.* **1988**, *60*, 2800−2803.
(53) Tolédano, P.; Krexner, G.; Prem, M.; Weber, H.-P.; Dmitriev, V. P. Theory of the martensitic transformation in cobalt. *Phys. Rev. B: Condens. Matter Mater. Phys.* **2001**, *64*, 144104.
(54) Orikasa, Y.; Maeda, T.; Koyama, Y.; Murayama, H.; Fukuda, K.; Tanida, H.; Arai, H.; Matsubara, E.; Uchimoto, Y.; Ogumi, Z. Direct Observation of a Metastable Crystal Phase of Li_xFePO_4 under Electrochemical Phase Transition. *J. Am. Chem. Soc.* **2013**, *135*, 5497−5500.
(55) Gremaud, R.; Broedersz, C. P.; Borsa, D. M.; Borgschulte, A.; Mauron, P.; Schreuders, H.; Rector, J. H.; Dam, B.; Griessen, R. Hydrogenography: An Optical Combinatorial Method To Find New Light-Weight Hydrogen-Storage Materials. *Adv. Mater.* **2007**, *19*, 2813−2817.

https://dx.doi.org/10.1021/acs.inorgchem.0c00059
Inorg. Chem. 2020, 59, 6800−6807